

THE PECULIAR TYPE IB SUPERNOVA 2006JC: A WCO WOLF-RAYET STAR EXPLOSION

N. TOMINAGA^{1,2}, M. LIMONGI^{3,2,4}, T. SUZUKI², M. TANAKA², K. NOMOTO^{5,2}, K. MAEDA^{5,6}, A. CHIEFFI⁷, A. TORNAMBE³,
T. MINEZAKI⁸, Y. YOSHII⁸, I. SAKON², T. WADA⁹, Y. OHYAMA⁹, T. TANABÉ⁹, H. KANEDA⁹, T. ONAKA², T. NOZAWA¹⁰,
T. KOZASA¹⁰, K. S. KAWABATA¹¹, G. C. ANUPAMA¹², D.K. SAHU¹², U.K. GURUGUBELLI¹², T.P. PRABHU¹², AND J. DENG¹³

Accepted for publication in the Astrophysical Journal.

ABSTRACT

We present a theoretical model for Type Ib supernova (SN) 2006jc. We calculate the evolution of the progenitor star, hydrodynamics and nucleosynthesis of the SN explosion, and the SN bolometric light curve (LC). The synthetic bolometric LC is compared with the observed bolometric LC constructed by integrating the UV, optical, near-infrared (NIR), and mid-infrared (MIR) fluxes. The progenitor is assumed to be as massive as $40M_{\odot}$ on the zero-age main-sequence. The star undergoes extensive mass loss to reduce its mass down to as small as $6.9M_{\odot}$, thus becoming a WCO Wolf-Rayet star. The WCO star model has a thick carbon-rich layer, in which amorphous carbon grains can be formed. This could explain the NIR brightening and the dust feature seen in the MIR spectrum. We suggest that the progenitor of SN 2006jc is a WCO Wolf-Rayet star having undergone strong mass loss and such massive stars are the important sites of dust formation. We derive the parameters of the explosion model in order to reproduce the bolometric LC of SN 2006jc by the radioactive decays: the ejecta mass $4.9M_{\odot}$, supernova-like explosion energy 10^{52} ergs, and ejected ^{56}Ni mass $0.22M_{\odot}$. We also calculate the circumstellar interaction and find that a CSM with a flat density structure is required to reproduce the X-ray LC of SN 2006jc. This suggests a drastic change of the mass-loss rate and/or the wind velocity that is consistent with the past luminous blue variable (LBV)-like event.

Subject headings: dust, extinction — infrared: ISM — nuclear reactions, nucleosynthesis, abundances — supernovae: general — supernovae: individual (SN 2006jc) — stars: Wolf-Rayet

1. INTRODUCTION

On 9th October 2006, Nakano et al. (2006) reported K. Itagaki's discovery of a possible supernova (SN) in UGC 4904. Although the SN was discovered after the peak, an upper limit of the R magnitude ($M_R > -12.2$) was obtained at ~ 20 days before the discovery (Pastorello et al. 2007). Interestingly, Nakano et al. (2006) also reported that an optical transient had appeared in 2004 close to the position of SN 2006jc. The transient was as faint as $M_R \sim -14$ and its duration

was as short as ~ 10 days. Since the event was faint and short-lived, they speculated that the transient was a luminous blue variable (LBV)-like event. The spatial coincidence between the LBV-like event and SN 2006jc is confirmed by Pastorello et al. (2007). Because of such an intriguing association with the LBV-like event, many groups performed follow-up observations of SN 2006jc in various wavebands: X-ray, ultra violet (UV), optical, infrared (IR), and radio.

Spectroscopic observations showed many broad features and strong narrow He I emission lines. According to the He detection, SN 2006jc was classified as Type Ib (Crotts et al. 2006; Fesen et al. 2006a; Benetti et al. 2006; Modjaz et al. 2006a,b). However, strange spectral features and their evolutions were reported. A bright blue continuum was prominent in the optical spectrum at early epochs (Foley et al. 2007; Pastorello et al. 2007; Smith et al. 2008). Such a bright blue continuum had also been observed in Type II SN 1988Z (Turatto et al. 1993), but the origin of this feature is still unclear. As the blue continuum declined, the red wing brightened and the optical spectra showed “U”-like shapes (Smith et al. 2008; Kawabata et al. 2008). This is a distinguishing feature of SN 2006jc in contrast to the spectra of usual SNe that have a peak in optical bands.

Photometric observations in optical and IR bands were performed continuously. The optical light curve (LC) showed a rapid decline from 50 days after the discovery, as in the case of SN 1999cq (Matheson et al. 2000). At the same epoch, near infrared (NIR) emissions brightened (Arkharov et al. 2006; Di Carlo et al. 2007). The NIR brightness increased from ~ 40 days to ~ 70 days after the discovery and then declined (Di Carlo et al. 2007). The epoch of the NIR brightening corresponds

¹ Optical and Infrared Astronomy Division, National Astronomical Observatory, 2-21-1 Osawa, Mitaka, Tokyo, Japan; nozomu.tominaga@nao.ac.jp

² Department of Astronomy, School of Science, University of Tokyo, 7-3-1 Hongo, Bunkyo-ku, Tokyo, Japan

³ Istituto Nazionale di Astrofisica - Osservatorio Astronomico di Roma, Via Frascati 33, I-00040, Monteporzio Catone, Italy

⁴ Center for Stellar and Planetary Astrophysics, School of Mathematical Sciences, P.O. Box, 28M, Monash University, Victoria 3800, Australia

⁵ Institute for the Physics and Mathematics of the Universe, University of Tokyo, Kashiwa, Chiba, Japan

⁶ Max-Planck-Institut für Astrophysik, Karl-Schwarzschild Strasse 1, 85741 Garching, Germany

⁷ Istituto Nazionale di Astrofisica - Istituto di Astrofisica Spaziale e Fisica Cosmica, Via Fosso del Cavaliere 100, Roma, Italy

⁸ Institute of Astronomy, School of Science, University of Tokyo, 2-21-1 Osawa, Mitaka, Tokyo, Japan

⁹ Institute of Space and Astronautical Science, Japan Aerospace Exploration Agency, 3-1-1 Yoshinodai, Sagamihara, Kanagawa, Japan

¹⁰ Department of Cosmosciences, Graduate School of Science, Hokkaido University, Sapporo, Japan

¹¹ Hiroshima Astrophysical Science Center, Hiroshima University, Hiroshima, Japan

¹² Indian Institute of Astrophysics, Bangalore, 560 034, India

¹³ National Astronomical Observatories, Chinese Academy of Sciences, Beijing 100012, China

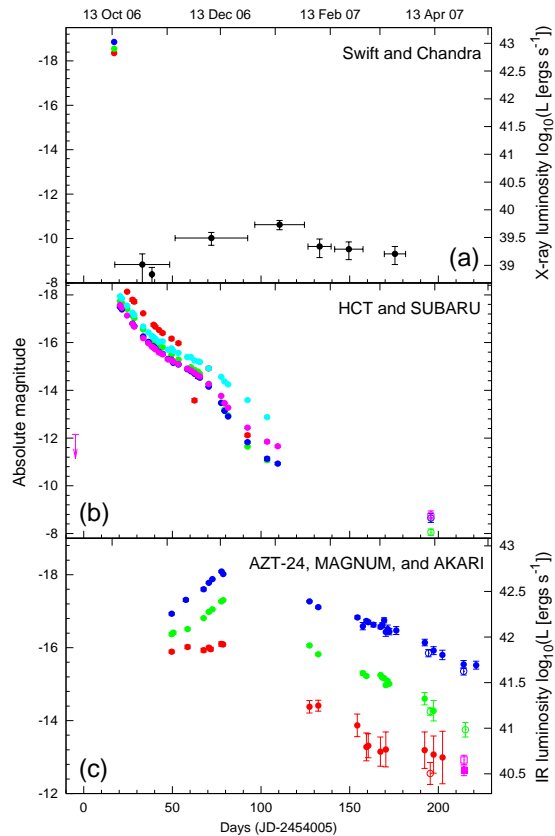


FIG. 1.— Multicolor available observations of SN 2006jc. (a) X-ray and UV luminosities obtained with the *Swift* and *Chandra* satellites (*black*: X-ray, *red*: UVW2-band, *green*: UVM2-band, *blue*: UVW1-band, Immler et al. 2008). X-ray LC is shown in a unit of ergs s^{-1} (right axis). (b) Optical luminosities obtained with the *HCT* telescope (*filled*, Anupama et al. 2008) and the *SUBARU* telescope (*open*, Kawabata et al. 2007a, 2008). The upper limit is taken from Pastorello et al. (2007). The color represents the wavelengths (U-band: *red*, B-band: *green*, V-band: *blue*, R-band: *magenta*, I-band: *cyan*). (c) IR luminosities obtained with the *AZT-24* telescope (*filled circles*, Arkharov et al. 2006; Di Carlo et al. 2007), the *MAGNUM* telescope (*open circles*, Minezaki et al. 2007), and the *AKARI* satellite (*squares*, Sakon et al. 2007). The color of circles represents the wavelengths (J-band: *red*, H-band: *green*, and K-band: *blue*). The contributions to the IR luminosities from the hot dust (*filled square*) and with the hot and warm dust (*open square*) are shown in a unit of ergs s^{-1} (right axis).

to that of the development of the red wing in the optical spectra (Smith et al. 2008).

The NIR brightening, as well as the fact that the redder side of the He emission profile declined faster than the bluer side, has been interpreted as an evidence of an ongoing dust formation (Smith et al. 2008). Additionally, on 29th April 2007 (200 days after the discovery), the *AKARI* satellite performed NIR and mid-infrared (MIR) photometric and spectroscopic observations (Sakon et al. 2007) and the *MAGNUM* telescope obtained the NIR photometries (Minezaki et al. 2007). They report the formation of amorphous carbon dust: another piece of evidences of the dust formation.

X-ray and UV emissions have also been observed by the *Swift* and *Chandra* satellites (Brown et al. 2006; Immler et al. 2006, 2008; Holland et al. 2007). X-ray observations were performed at seven epochs and showed a brightening from ~ 20 days to ~ 100 days after the discovery (Brown et al. 2006; Immler et al. 2006, 2008).

TABLE 1
OPTICAL LUMINOSITIES.

Date [JD-2454005]	L_{opt} [$10^{40} \text{ergs s}^{-1}$]
20	370
21	340
24	250
27	180
28	170
33	110
36	87
38	75
39	70
40	66
42	58
44	53
47	44
49	40
53	36
58	28
60	27
62	25
64	23
65	22
70	15
77	6.3
79	4.8
81	4.0
89	2.2
92	2.1
103	1.0
119	0.36
138	0.23
195	0.15

The X-ray detection suggests an interaction between the SN ejecta and the circumstellar matter (CSM). On the contrary, the radio emission was not detected by Very Large Array (VLA) (Soderberg 2006).

We present a SN explosion model of a Wolf-Rayet star that explains the bolometric and X-ray LCs. Hydrodynamics, nucleosynthesis, and LC synthesis calculations are performed assuming the spherical symmetry. In this study, we assume the explosion date of SN 2006jc to be 15 days before the discovery ($t = 0$) and the energy source of the light to be the ^{56}Ni - ^{56}Co decay.

The paper is organized as follows: in § 2, we describe how we derive the bolometric LC from observations in the various wavebands, in § 3, we briefly discuss the pre-supernova evolutionary properties of the progenitor star; in § 4, hydrodynamical and nucleosynthesis calculations are described; in § 5, LC synthesis calculations are presented; in § 6, we calculate the X-ray emission due to the ejecta-CSM interaction; in § 7 and § 8, conclusions and discussion are presented.

2. PHOTOMETRIC OBSERVATIONS AND BOLOMETRIC LIGHT CURVE

The bolometric luminosities of SNe are usually estimated from the integration over the optical and NIR emission because the usual SNe radiate dominantly in the optical and NIR bands (e.g., Yoshii et al. 2003; Minezaki et al. 2008). However, the spectra of SN 2006jc show the bright red and blue wings (Smith et al. 2008; Kawabata et al. 2008; Anupama et al. 2008), which implies that the emissions in UV and IR bands considerably contribute to the bolometric luminosity.

We construct the bolometric luminosity with the inte-

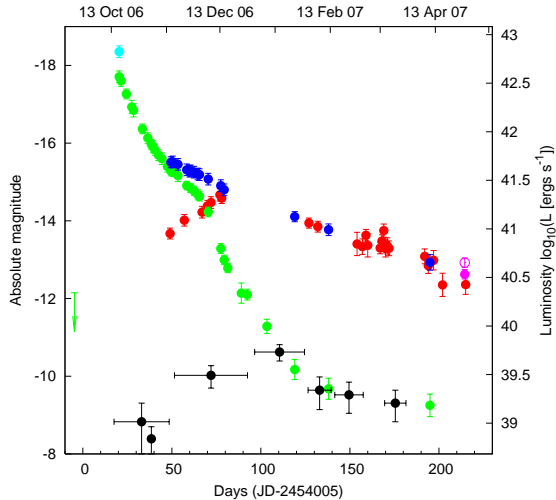


FIG. 2.— Comparison of multicolor LCs of SN 2006jc (L_{opt} : green filled circles, Kawabata et al. 2007a, 2008; Anupama et al. 2008; $L_{\text{UV}} + L_{\text{opt}}$: cyan filled circles, Immler et al. 2008; Anupama et al. 2008; $L_{\text{IR,est}}(\nu < 3 \times 10^{14}\text{Hz})$: red filled circles, Arkharov et al. 2006; Di Carlo et al. 2007; $L_{\text{opt}} + L_{\text{IR,est}}(\nu < 3 \times 10^{14}\text{Hz})$: blue filled circles, Kawabata et al. 2007a, 2008; Anupama et al. 2008; Arkharov et al. 2006; Di Carlo et al. 2007; $L_{\text{IR,hot}}(\nu < 3 \times 10^{14}\text{Hz})$: magenta filled circle, Sakon et al. 2007; $L_{\text{IR}}(\nu < 3 \times 10^{14}\text{Hz})$: magenta open circle, Sakon et al. 2007; and L_{X} : black filled circles, Immler et al. 2008).

gration of the UV, optical, and IR photometries that are obtained with the *HCT* (Anupama et al. 2008), *AZT-24* (Arkharov et al. 2006; Di Carlo et al. 2007), *MAGNUM* (Minezaki et al. 2007), and *SUBARU* telescopes (Kawabata et al. 2007a, 2008) and the *Swift* (Immler et al. 2008) and *AKARI* satellites (Sakon et al. 2007). Since the UV fluxes are available only at $t = 17$ days (Immler et al. 2008), the UV luminosity is estimated from the optical luminosity at the other epoch. Available observations are shown in Figure 1. Details of optical observations will be presented in the forthcoming papers (e.g., Anupama et al. 2008; Kawabata et al. 2008). We adopt a distance of 25.8Mpc corresponding to a distance modulus of 32.05 (Pastorello et al. 2007) and a reddening of $E(B - V) = 0.05$ (Schlegel et al. 1998; Pastorello et al. 2007).

2.1. Optical emission

The optical LCs were obtained with the *HCT* and *SUBARU* telescopes (Kawabata et al. 2007a, 2008; Anupama et al. 2008). We integrate the optical fluxes with a cubic spline interpolation from 3×10^{14} Hz to 1×10^{15} Hz. The optical luminosities (L_{opt}) are summarized in Table 1 and the LC is shown in Figure 2. The optical LC declines monotonically after the discovery. The decline suddenly becomes rapid at $t > 70$ days and the optical luminosity finally goes down to $L_{\text{opt}} \sim 10^{39}\text{ergs s}^{-1}$ at $t \sim 200$ days.

The X-ray LC obtained with the *Swift* and *Chandra* satellites (Immler et al. 2008) shows that the X-ray luminosities, L_{X} , are much fainter than the optical luminosities (Brown et al. 2006; Immler et al. 2006, 2008). Thus, the X-ray contribution to the bolometric luminosities is negligible. However, the UV luminosity, L_{UV} , is comparable to the optical luminosity at $t = 17$ days ($L_{\text{UV}} \sim 3 \times 10^{42}\text{ergs s}^{-1}$ as estimated from the UVOT

observations, Immler et al. 2008).¹⁴ The UV luminosity is $\sim 80\%$ of the optical luminosity, i.e., the total flux is ~ 1.8 times brighter than the optical flux (Fig. 2). Since the UV flux declined as the optical flux (Holland et al. 2007), we assume that $L_{\text{UV}} \sim 0.8L_{\text{opt}}$ at every epoch. Although the blue wing declines with time and L_{UV} might be over-estimated at $t \gtrsim 90$ days (Smith et al. 2008), the bolometric luminosity (L_{bol}) should be reliable because the IR contribution dominates in the bolometric luminosity at such late epochs (§ 2.2).

2.2. Infrared emission

The IR spectroscopy and photometries are obtained with the *AZT-24* and *MAGNUM* telescopes (NIR photometries, Arkharov et al. 2006; Di Carlo et al. 2007; Minezaki et al. 2007) and the *AKARI* satellite (NIR spectroscopy and MIR photometries, Sakon et al. 2007). As indicated by the red wing in the optical spectra, the IR emission considerably contributes to the bolometric luminosity of SN 2006jc.

The MIR observation is available at $t = 215$ days (Sakon et al. 2007). The IR luminosity integrated over $\nu < 3 \times 10^{14}$ Hz is estimated from the NIR and MIR observations as $L_{\text{IR}}(\nu < 3 \times 10^{14}\text{Hz}) = 4.5 \times 10^{40}$ ergs s^{-1} . Sakon et al. (2007) concluded that the IR emission is originated from amorphous carbon grains with two temperatures of $T = 800\text{K}$ and 320K . The large difference between the two temperatures would imply that the origin of the hot carbon dust with $T = 800\text{K}$ is different from that of the warm carbon dust with $T = 320\text{K}$. The hot carbon dust is suggested to be newly formed in the SN ejecta and heated by the ^{56}Ni - ^{56}Co decay by a dust formation calculation (Nozawa et al. 2008). On the other hand, the origin of the emission from the warm carbon dust is suggested to be a SN light echo of the CSM carbon dust (Sakon et al. 2007; Mattila et al. 2008; see also Nozawa et al. 2008). Therefore, we assume that the optical emission from SN 2006jc is absorbed and simultaneously re-emitted by the hot carbon dust and thus the luminosity emitted from the hot carbon dust should be included in the bolometric luminosity of SN 2006jc. According to the estimated temperatures and masses of the hot and warm carbon grains (Sakon et al. 2007), the luminosities contributed by the hot and warm carbon grains are $L_{\text{IR,hot}}(\nu < 3 \times 10^{14}\text{Hz}) = 3.2 \times 10^{40}$ ergs s^{-1} and $L_{\text{IR,warm}}(\nu < 3 \times 10^{14}\text{Hz}) = 1.1 \times 10^{40}$ ergs s^{-1} , respectively.¹⁵

For the epochs when the IR photometries at $\nu < 1.3 \times 10^{14}\text{Hz}$ are unavailable, we estimate the contribution of the IR emission by fitting the JHK-band photometries with amorphous carbon emission.

From the Kirchhoff's law, the thermal radiation from a spherical dust grain X with a uniform radius a_{X} and temperature T_{X} is given by $4\pi a_{\text{X}}^2 B(\nu, T_{\text{X}}) Q_{\text{X}}^{\text{abs}}(\nu)$, where $Q_{\text{X}}^{\text{abs}}(\nu)$ is the absorption efficiency of the grain. For the optically thin case, the observed emission from dust

¹⁴ The UV flux is estimated using the *Swift* UVOT calibration documents (<http://swift.gsfc.nasa.gov/docs/swift/swiftsc.html>).

¹⁵ The difference between $L_{\text{IR}}(\nu < 3 \times 10^{14}\text{Hz})$ and $L_{\text{IR,hot}}(\nu < 3 \times 10^{14}\text{Hz}) + L_{\text{IR,warm}}(\nu < 3 \times 10^{14}\text{Hz})$ stems from that the H-band luminosity is slightly brighter than the luminosity emitted from the hot carbon dust (Sakon et al. 2007).

TABLE 2
PARAMETERS FOR AMORPHOUS CARBON FITTING OF THE JHK-BAND PHOTOMETRIES AND
THE ESTIMATED IR LUMINOSITIES.

Date [JD-2454005]	C_ϵ [10^{34}]	$T_{C,\text{hot}}$ [K]	$L_{\text{IR,est}}(\nu < 1.3 \times 10^{14} \text{Hz})$ [$10^{40} \text{ergs s}^{-1}$]	$L_{\text{IR,est}}(\nu < 3 \times 10^{14} \text{Hz})$ [$10^{40} \text{ergs s}^{-1}$]
49	3.9	1580	2.9	9.0
57	12	1330	5.1	12
67	16	1340	6.6	15
70	19	1330	7.8	17
72	23	1300	8.9	19
77	27	1310	11	23
79	18	1400	9.1	21
127	46	1050	7.6	12
132	52	1010	7.2	11
154	17	1150	4.2	7.0
157	32	1010	4.5	6.6
159	75	900	6.7	8.7
160	26	1050	4.4	6.8
167	35	990	4.5	6.4
168	54	940	5.5	7.5
169	99	880	7.6	9.7
170	48	930	4.8	6.3
171	45	950	4.9	6.7
172	44	940	4.6	6.3
192	48	900	4.0	5.3
195	45	870	3.3	4.2
197	56	860	3.8	4.8
202	5.6	1190	1.5	2.7
215	28	870	2.1	2.7

grains X is written as

$$f_X(\nu) = N_X \pi B(\nu, T_X) Q_X^{\text{abs}}(\nu) \left(\frac{a_X}{R} \right)^2, \quad (1)$$

where N_X and R denote the total number of the dust particles and the distance from the observer, respectively (Sakon et al. 2007). In the followings, we convolve the ν -independent coefficients as an emission coefficient $C_\epsilon = \pi N_X (a_X/R)^2$. Applying the absorption efficiency for the amorphous carbon grain with $a_C = 0.01 \mu\text{m}$, we derive the temperature of the hot carbon dust, $T_{C,\text{hot}}$, and C_ϵ to reproduce the JHK-band photometries.

To justify the above estimate, we compare the estimate with the actual MIR observation at $t = 215$ days (Sakon et al. 2007). The fitting gives the temperature $T_{C,\text{hot}} = 870$ K and the emission coefficient $C_\epsilon = 2.8 \times 10^{35}$ for the HK-band photometries at $t = 215$ days. The luminosity integrated over $\nu < 3 \times 10^{14} \text{Hz}$ is $L_{\text{IR,est}}(\nu < 3 \times 10^{14} \text{Hz}) = 2.7 \times 10^{40} \text{ergs s}^{-1}$. The temperature and luminosity are roughly consistent with those of the hot carbon dust. The agreement indicates that the fitting gives a good estimate of the IR emission due to the hot carbon dust. We note that the estimate can not account for the emission from the warm carbon dust.

Table 2 summarizes the emission coefficient, temperature, estimated luminosity at $\nu < 1.3 \times 10^{14} \text{Hz}$, and luminosity emitted below $\nu = 3 \times 10^{14} \text{Hz}$. The dust temperature roughly declines from $T_{C,\text{hot}} \sim 1600 \text{K}$ at $t = 49$ days to $T_{C,\text{hot}} \sim 870 \text{K}$ at $t = 215$ days. This is consistent with a picture that the hot carbon dust was formed in the SN ejecta and cooled down gradually (Nozawa et al. 2008). The IR LC is shown in Figure 2. The estimated luminosity at $\nu < 1.3 \times 10^{14} \text{Hz}$ evolves as the JHK LCs, and thus the IR LC brightens at $t \sim 50 - 80$ days and declines at $t > 120$ days. Since there is no NIR data

TABLE 3
BOLOMETRIC LUMINOSITIES.

Date [JD-2454005]	L_{bol} [$10^{40} \text{ergs s}^{-1}$]
49	81
51	81
53	75
58	64
60	61
62	59
65	55
66	54
70	45
77	33
79	29
119	14
138	10
195	4.7

at $t \sim 80 - 120$ days, the bolometric LC can not be estimated at this epoch. The bolometric luminosity is derived from the summation of L_{UV} , L_{opt} , and L_{IR} and summarized in Table 3, where $L_{\text{UV}} = 0.8 L_{\text{opt}}$ is applied.

3. THE PROGENITOR STAR

The presupernova model has been extracted from a set of models already presented by Limongi & Chieffi (2006) and computed with the latest release of the stellar evolutionary code FRANEC (5.050218). Since all the features of this code have been already presented, we will address here only the main points. The interaction between convection and local nuclear burning has been taken into account by coupling together and solving simultaneously the set of equations governing the chemical evolution due to the nuclear reactions and those describing the convective mixing. More specifically, the convective mixing has been treated by means of a diffusion equation where the

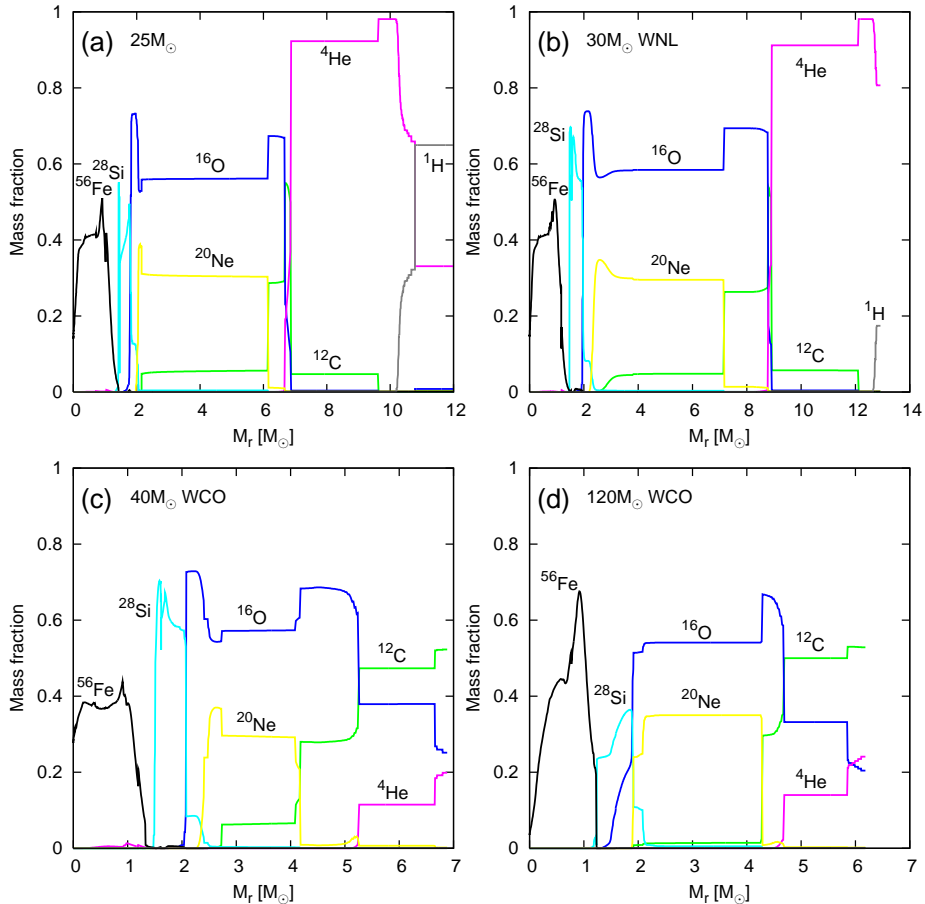


FIG. 3.— Abundance distributions of presupernova models with (a) $M_{\text{ms}} = 25M_{\odot}$, (b) $M_{\text{ms}} = 30M_{\odot}$, (c) $M_{\text{ms}} = 40M_{\odot}$, and (d) $M_{\text{ms}} = 120M_{\odot}$. Note that the chemical composition of the outmost layer is C rich in the WCO Wolf-Rayet stars (c,d).

diffusion coefficient is computed by the use of the mixing-length theory. The nuclear network is the same as that adopted in Limongi & Chieffi (2003), but the nuclear cross sections have been updated whenever possible (see Table 1 in Limongi & Chieffi 2006). A moderate amount of overshooting of $0.2 H_{\text{p}}$ has been included into the calculation only on the top of the convective core during core H burning. Mass loss has been taken into account following the prescriptions of Vink et al. (2000) for the blue supergiant phase ($T_{\text{eff}} > 12000\text{K}$), de Jager et al. (1988) for the red supergiant phase ($T_{\text{eff}} < 12000\text{K}$), Nugis & Lamers (2000) for the WNE/WCO Wolf-Rayet phase and Langer (1989) during the WNE/WCO Wolf-Rayet phases. We adopt the following correspondence of the models to the various WR phases according to the surface abundances, as suggested by Maeder & Meynet (2003): WNL ($10^{-5} < X(\text{H})_{\text{surf}} < 0.4$), WNE ($X(\text{H})_{\text{surf}} < 10^{-5}$ and $(\text{C}/\text{N})_{\text{surf}} < 0.1$), WNC ($0.1 < (\text{C}/\text{N})_{\text{surf}} < 10$) and WCO ($(\text{C}/\text{N})_{\text{surf}} > 10$). (Hereafter, C/N and C/O denote the number ratios.)

The X-ray emission, as well as the early bright blue continuum and the narrow He I lines, clearly indicates an interaction between the SN ejecta and the CSM, i.e., the existence of a dense CSM. Furthermore, the IR spectral energy distribution may be explained by the formation of amorphous carbon grains in the SN ejecta and the CSM (Sakon et al. 2007, see also Nozawa et al. 2008). Since the C-rich environment (i.e., $\text{C}/\text{O} > 1$) is required to form carbon dust (e.g., Nozawa et al. 2003), the IR

observations suggest that the SN ejecta and CSM contain a C-rich layer. This suggests that the progenitor star of SN 2006jc is a WCO Wolf-Rayet star with a C-rich envelope and CSM (Figs. 3a-3d).

Inspection of all the presupernova models available in Limongi & Chieffi (2006) indicates that only massive models, i.e., $M_{\text{ms}} > 40M_{\odot}$, fulfill the requirements from the IR observation and become WCO stars. Moreover, these are the only stars in which the chemical compositions of the mantle and CSM are dominated mainly by C with a smaller amount of O (Fig. 3cd).

In stars with initial masses smaller than $M_{\text{ms}} \sim 35M_{\odot}$, the mass of the He convective core increases or remains constant during the core He burning phase. At core He exhaustion, a sharp discontinuity of He abundance is produced at the outer edge of the CO core. Then, the CO core begins to contract to ignite the next nuclear fuel while He burning shifts to a shell inducing a formation of a convective zone. The He convective shell forms beyond the He discontinuity at the outer edge of the CO core. Hence its chemical composition is dominated by He [$X(\text{He}) > 0.9$]. Because of the short lifetime of the advanced burning stages, only a small amount of He is burned inside the shell before the presupernova stage (Figs. 3ab). Such a behavior is typical for stars in which the He core mass remains roughly constant during core He burning (e.g., Nomoto & Hashimoto 1988).

In stars with initial masses greater than $M_{\text{ms}} \sim 35M_{\odot}$, on the contrary, the mass loss is efficient enough (10^{-5} –

TABLE 4
BASIC EVOLUTIONARY PROPERTIES OF THE
PROGENITOR STAR.

Key quantities	
H Burning	
t_{H} [Myr]	4.64
M_{CC} [M_{\odot}]	25.80
M_{tot} [M_{\odot}]	35.40
t_{O} [Myr]	4.16
M_{He} [M_{\odot}]	10.01
He Burning	
t_{He} [Myr]	0.46
$M_{\text{He,CC}}$ [M_{\odot}]	12.56
M_{tot} [M_{\odot}]	7.04
M_{env} [M_{\odot}]	18.80
$X(^{12}\text{C})_{\text{cen}}$	0.28
t_{red} [Myr]	0.07
t_{WNL} [Myr] ($X(\text{He})_{\text{cen}}$)	0.11 (0.77)
t_{WNE} [Myr] ($X(\text{He})_{\text{cen}}$)	0.054 (0.44)
t_{WCO} [Myr] ($X(\text{He})_{\text{cen}}$)	0.21 (0.31)
Advanced Burnings	
Δt_{exp} [yr]	1.25(+4)
$M_{\text{He(max)}}$ [M_{\odot}]	16.52
$M_{\text{CO(max)}}$ [M_{\odot}]	4.83
$M_{\text{Fe,preSN}}$ [M_{\odot}]	1.50
M_{preSN} [M_{\odot}]	6.88
R_{preSN} [cm]	3.08(+10)
$M_r(\text{He}_{\text{shell}})$ (Int.-Ext.) [M_{\odot}]	5.262-6.648
$M_r(\text{C}_{\text{shell}})$ (Int.-Ext.) [M_{\odot}]	2.736-4.097
$t_{\text{WNL(tot)}}$ [yr]	1.10(+5)
$t_{\text{WNE(tot)}}$ [yr]	5.43(+4)
$t_{\text{WCO(tot)}}$ [yr]	2.21(+5)
$t_{\text{WR(tot)}}$ [yr]	3.86(+5)

$10^{-4}M_{\odot} \text{ yr}^{-1}$) to uncover the He core and they reduce progressively their mass during the core He burning phase. The star enters the WNE Wolf-Rayet stage and its subsequent evolution is governed by the actual size of the He core. In particular, as the He core progressively reduces due to the mass loss, the star tends to behave as an initially-lower mass star, i.e., essentially reduces its central temperature. This induces the He convective core to shrink progressively in mass as well, leaving a layer with a variable chemical composition that reflects the central abundances at various stages during core He burning. When the stellar mass is reduced below the maximum extension of the He convective core, the products of core He burning appear on the surface and the star becomes a WCO Wolf-Rayet star. At core He exhaustion, He burning shifts to a shell inducing the formation of the convective shell. The convective shell forms in the region with variable chemical composition. As a consequence, at variance with what happens in stars with $M_{\text{ms}} \lesssim 35M_{\odot}$, in these stars, the chemical composition of the convective shell becomes a mixture of the central He burning products. Hence it is mainly composed of C, O and He (Figs. 3cd).

Since all the models above $40 M_{\odot}$ have a similar presupernova structure, we selected a $40 M_{\odot}$ star as representative of a typical star becoming a WCO Wolf-Rayet star. The mass at the presupernova stage (M_{preSN}) is $M_{\text{preSN}} = 6.9M_{\odot}$ because of the strong mass loss. We

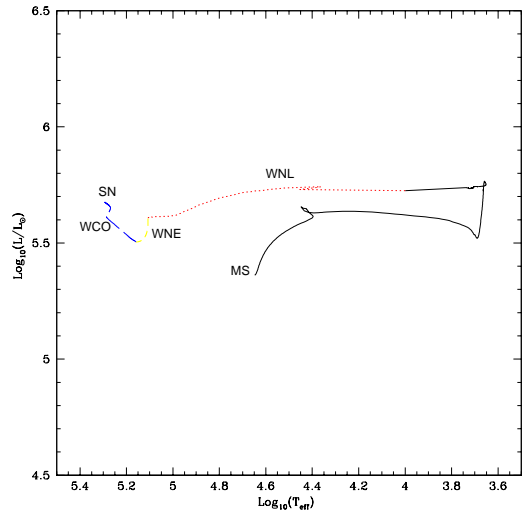


FIG. 4.— Presupernova evolutionary path of the progenitor star with $M_{\text{ms}} = 40M_{\odot}$ in the Hertzsprung-Russell diagram.

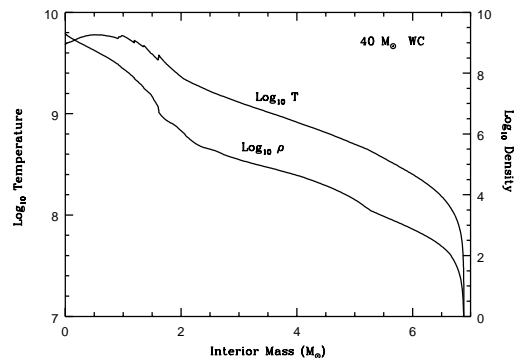


FIG. 5.— Temperature and density structures of the presupernova progenitor star with $M_{\text{ms}} = 40M_{\odot}$.

underline that the $M_{\text{ms}}-M_{\text{preSN}}$ relation is highly uncertain because it strongly depends on many details of the stellar evolution (e.g., the mass loss, overshooting, rotation, and metallicity, see Langer 1989; Nugis & Lamers 2000; Meynet & Maeder 2003; Nomoto et al. 2006; Limongi & Chieffi 2006; Eldridge & Vink 2006). For this reason, for the purpose of this study, we mainly focus on a WCO progenitor with $M_{\text{preSN}} \sim 6.9 M_{\odot}$, without paying much emphasis on M_{ms} .

A detailed discussion of the presupernova evolution during all the nuclear burning stages is beyond the purpose of this paper. Hence we report here in Table 4 some key properties during the H, He, and advanced burning stages. In particular, for the H burning stage we report the following quantities: the H burning lifetime (t_{H}), the maximum extension of the convective core (M_{CC}), the total mass (M_{tot}) at core H exhaustion, the time spent as an O-type star (t_{O}) and the He core mass (M_{He}) at H exhaustion. Here, we assume that the temperature

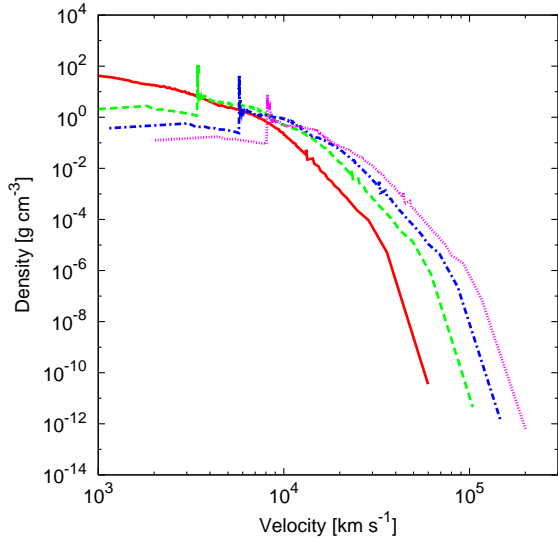


FIG. 6.— Density structures at 100 s after the explosions for the models with $E_{51} = 1$ (solid), $E_{51} = 5$ (dashed), $E_{51} = 10$ (dash-dotted), and $E_{51} = 20$ (dotted).

of the O-type stars is $33000 \text{ K} < T_{\text{eff}} < 50000 \text{ K}$. For the He burning phase we report the following quantities: the He burning lifetime (t_{He}), the maximum size of the He convective core ($M_{\text{He,CC}}$), M_{tot} at core He exhaustion, the maximum depth of the convective envelope (M_{env}), the central ^{12}C mass fraction at core He exhaustion [$X(^{12}\text{C})_{\text{cen}}$], the time spent at the red side ($\log T_{\text{eff}} < 3.8$) of the HR diagram (t_{red}), and the WNL, WNE, and WCO lifetimes (t_{WNL} , t_{WNE} , and t_{WCO} , respectively) - in parenthesis the central He mass fraction [$X(\text{He})_{\text{cen}}$] when the star enters the WNL, WNE and WCO phases. For the advanced burning stage we report the following key quantities: the time until the explosion (Δt_{exp}), the maximum size of the He core [$M_{\text{He}}(\text{max})$], the maximum size of the CO core [$M_{\text{CO}}(\text{max})$], the masses of the iron core ($M_{\text{Fe,preSN}}$) and the star (M_{preSN}) and the radius of the star (R_{preSN}) at the presupernova stage, the final extension in mass of the He convective shell [$M_r(\text{He}_{\text{shell}})$] and of the convective C shell [$M_r(\text{C}_{\text{shell}})$], and the total lifetimes during the WNL [$t_{\text{WNL}}(\text{tot})$], WNE [$t_{\text{WNE}}(\text{tot})$], WCO [$t_{\text{WCO}}(\text{tot})$], and WR [$t_{\text{WR}}(\text{tot})$, where $t_{\text{WR}} = t_{\text{WNL}} + t_{\text{WNE}} + t_{\text{WCO}}$] phases.

Figures 4 and 5 show the evolutionary path in the HR diagram and the temperature and density profiles at the presupernova stage.

4. HYDRODYNAMICS AND NUCLEOSYNTHESIS

The SN explosion and explosive nucleosynthesis are calculated for the progenitor star with $M_{\text{preSN}} = 6.9M_{\odot}$. We apply various explosion energies ($E_{51} = E/10^{51} \text{ ergs} = 1, 5, 10, \text{ and } 20$) for the SN explosion calculations (e.g., Nomoto et al. 2006; Tominaga et al. 2007b). The hydrodynamical calculation is performed by means of a spherical Lagrangian hydrodynamics code with a piecewise parabolic method (PPM, Colella & Woodward 1984) including nuclear energy production from the α -network. The equation of state takes account of the gas, radiation, e^-e^+ pair (Sugimoto & Nomoto 1975), Coulomb interactions between ions and electrons, and phase transition (Nomoto et al. 1982; Nomoto & Hashimoto 1988). Af-

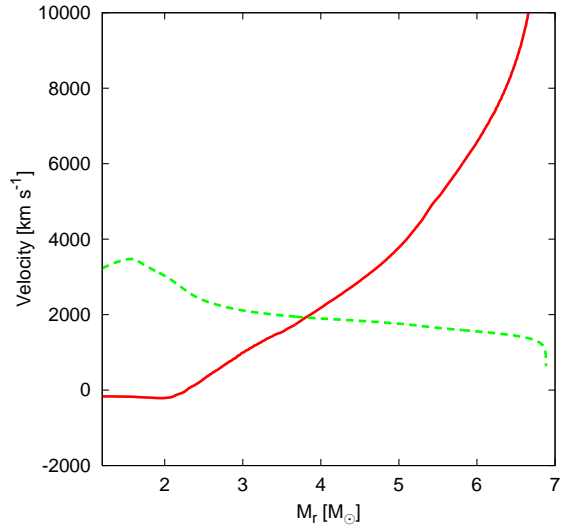


FIG. 7.— Comparison between an escape velocity (dashed) and an ejecta velocity for the model with $E_{51} = 1$ (solid).

ter the hydrodynamical calculations, nucleosynthesis is calculated as a post-processing with a reaction network that includes 280 isotopes up to ^{79}Br (see Table 1 in Umeda & Nomoto 2005).

Since the explosion mechanism of a core-collapse SN for a massive star with an iron core is still an unsolved problem (e.g., Janka et al. 2007), we initiate the SN explosion as a thermal bomb. Although there are various ways to simulate the explosion (e.g., a kinetic piston, Woosley & Weaver 1995), it is suggested that the explosive nucleosynthesis does not depend sensitively on the way how the explosion energy is deposited (Aufderheide et al. 1991). We set an inner reflective boundary at $M_r = 1M_{\odot}$ and $r = 1000 \text{ km}$ within the iron core and elevate temperatures at the inner boundary.

In the spherical symmetry case, for any given progenitor model, hydrodynamics and nucleosynthesis are determined by the explosion energy. During the SN explosion, a shock propagates outward inducing local compression and heating, triggering explosive nucleosynthesis. Behind the shock front the matter is accelerated and starts moving outward. However, if the progenitor has a deep gravitational potential and the explosion energy is low, the inner layers begin to fall back due to the gravitational attraction. A more compact star and a lower explosion energy leads a larger amount of fallback. The fallback has a deep implication on the SN nucleosynthesis because it decreases the matter ejection, especially, of the inner core (e.g., ^{56}Ni).

Figure 6 shows density structures at 100 s after the explosions when homologously expanding structures are reached ($v \propto r$). We find that the fallback takes place for the model with $E_{51} = 1$ but not for the models with $E_{51} = 5, 10, \text{ and } 20$. Figure 7 shows a comparison between the escape velocity and the ejecta velocity for the model with $E_{51} = 1$ and demonstrates that the matter below $M_r = M_{\text{fall}} = 3.8M_{\odot}$ will fall back. On the other hand, in the models with $E_{51} = 5, 10, \text{ and } 20$, the matter above the inner boundary will be ejected.

The abundance distributions after the explosions are shown in Figures 8a-8d. In every model, ^{58}Ni is synthesized in the innermost layer ($M_r < M_{\text{Fe,preSN}} = 1.5M_{\odot}$)

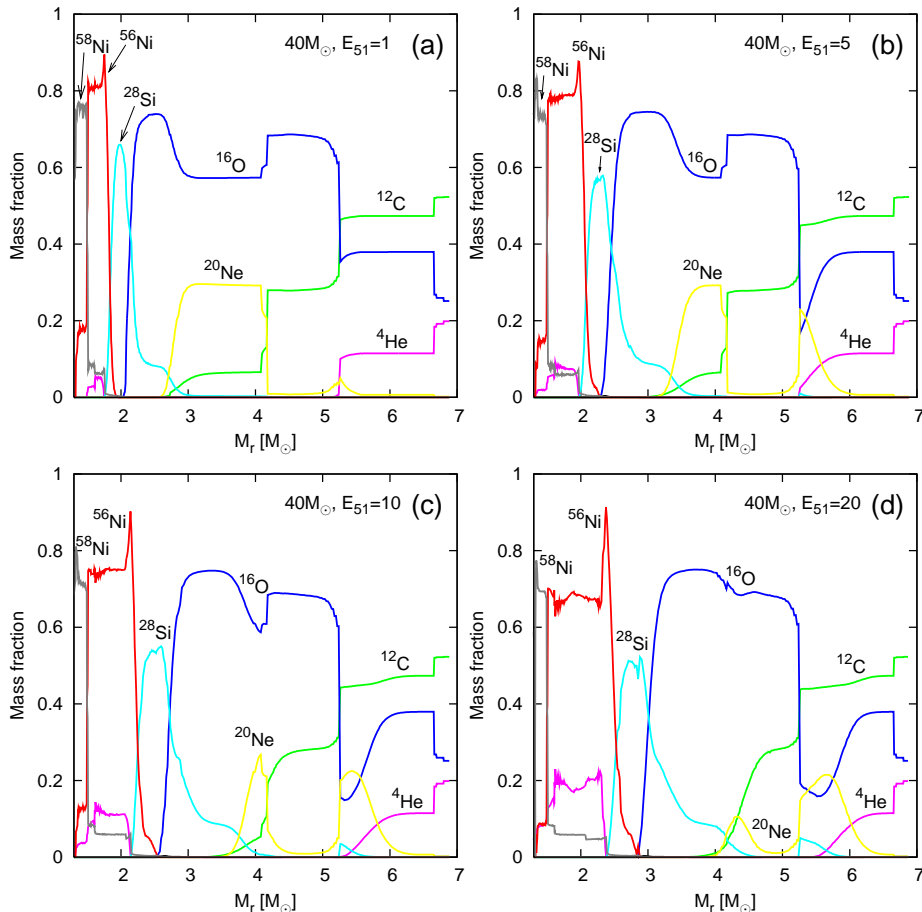


FIG. 8.— Abundance distributions after the explosions of the progenitor star with $M_{\text{ms}} = 40M_{\odot}$. The explosion energies are (a) $E_{51} = 1$, (b) $E_{51} = 5$, (c) $E_{51} = 10$, and (d) $E_{51} = 20$.

TABLE 5
NUCLEOSYNTHESIS PROPERTIES OF THE EXPLOSION
MODELS WITH $M_{\text{preSN}} = 6.9M_{\odot}$ ($M_{\text{ms}} = 40M_{\odot}$).

Explosion energy [10^{51} ergs]	M_{Fe} [M_{\odot}]	M_{Si} [M_{\odot}]	$M(^{56}\text{Ni})$ [M_{\odot}]	M_{cut} [M_{\odot}]
1	1.8	2.1	—	—
5	2.1	2.5	0.5	1.8
10	2.3	2.7	0.6	2.0
20	2.5	3.0	0.7	2.3

due to the low electron fraction. Thus, we can estimate the maximum amounts of synthesized ^{56}Ni for given energies. The ^{56}Ni -rich layer extending to $M_r = M_{\text{Fe}}$ [where $X(^{56}\text{Ni}) = X(^{28}\text{Si})$] and ^{28}Si -rich layer extending to $M_r = M_{\text{Si}}$ [where $X(^{28}\text{Si}) = X(^{16}\text{O})$] expand farther in the models with higher E because the temperature achieved is higher in the outer layer for higher E . M_{Fe} and M_{Si} for each model are summarized in Table 5.

^{56}Ni is synthesized at $M_r < M_{\text{Si}}$. Since $M_{\text{Si}} < M_{\text{fall}}$ in the model with $E_{51} = 1$, the model is likely not to eject ^{56}Ni . On the other hand, the models with $E_{51} = 5, 10$, and 20 can eject all synthesized ^{56}Ni because the fallback does not occur. The total amounts of synthesized ^{56}Ni for the models with $E_{51} = 5, 10$, and 20 are summarized in Table 5.

5. LIGHT CURVE

The energy source of the LC of SN 2006jc is still under debate. The possible sources include the ^{56}Ni - ^{56}Co decay like Type I SNe and the ejecta-CSM interaction like Type II In SNe. However, both scenarios have the following problems. In the case of the ^{56}Ni - ^{56}Co decay, the γ -ray photon and positron emitted from the ^{56}Ni - ^{56}Co decay are absorbed by the SN ejecta and the absorbed energy is thermalized. Thus, the spectra would show a blackbody-like continuum as normal Type I SNe do. However, the spectra of SN 2006jc do not resemble those of normal Type I SNe but show a bright blue continuum in early epochs (Foley et al. 2007; Smith et al. 2008). In the case of the ejecta-CSM interaction, the kinetic energy is transformed to an X-ray emission via bremsstrahlung radiation, and then converted to UV, optical, and IR emissions. Thus, it is difficult to explain that the X-ray luminosity is much fainter than the optical luminosity unless the optical depth for the X-ray emission is much higher than that for the optical emission. Another problem with the ejecta-CSM interaction model is that the X-ray LC is not synchronized with the bolometric LC. In addition, the LC powered by the ejecta-CSM interaction usually has a long-term plateau (e.g., SN 1997cy, Turatto et al. 2000). Thus, we assume that the LC is powered by the ^{56}Ni - ^{56}Co decay.

5.1. Radioactive Decay Models

The bolometric LC of SN 2006jc is constructed from the UV, optical, and IR observations as described in § 2. The estimated peak bolometric magnitude of SN 2006jc is $M = -18.4$, being as bright as SN 2006aj (e.g., Pian et al. 2006). Thus, it is speculated that the ejected amount of ^{56}Ni [$M(^{56}\text{Ni})$] is similar to SN 2006aj, i.e., $M(^{56}\text{Ni}) \sim 0.2M_{\odot}$ (Mazzali et al. 2006, 2007; Maeda et al. 2007). According to § 4, the models with $E_{51} = 5, 10,$ and 20 can eject a large enough amount of ^{56}Ni , while the ^{56}Ni production of the model with $E_{51} = 1$ is too small.

The spherical explosion models with $E_{51} = 5, 10,$ and 20 yield too much $M(^{56}\text{Ni})$ because of no fallback. However, no fallback is a consequence of the assumption of the spherical symmetry. The fallback takes place in an aspherical explosion even with a high explosion energy and thus the aspherical explosion may well decrease $M(^{56}\text{Ni})$ and increase the central remnant mass M_{rem} (Maeda & Nomoto 2003; Tominaga et al. 2007a; Tominaga 2007). Therefore, assuming that aspherical fallback takes place in the high-energy models with $E_{51} = 5, 10,$ and 20 , we estimate the amount of fallback to yield $M(^{56}\text{Ni}) \sim 0.2M_{\odot}$ and then the ejected masses for the models as $M_{\text{ej}} = M_{\text{preSN}} - M_{\text{rem}}$. As a result, the sets of $M_{\text{rem}}, M_{\text{ej}}$ and E are derived to be $(M_{\text{rem}}/M_{\odot}, M_{\text{ej}}/M_{\odot}, E_{51}) = (1.8, 5.1, 5), (2.0, 4.9, 10),$ and $(2.3, 4.6, 20)$.

Applying the homologous density structures of the models (Fig. 6), we synthesize bolometric LCs for the models with $E_{51} = 5, 10,$ and 20 using the LTE radiation hydrodynamics code and the gray γ -ray transfer code (Iwamoto et al. 2000). In the radiative transfer calculation, the electron scattering is calculated for the ionization states solved by the saha equation and the Rosseland mean opacity is approximated with an empirical relation to the electron-scattering opacity (Deng et al. 2005).

The peak width (τ) of the SN LC depends on the ejected mass M_{ej} , explosion energy E , opacity κ , density structure, and ^{56}Ni distribution, as $\tau \propto A\kappa^{1/2}M_{\text{ej}}^{3/4}E^{-1/4}$ (Arnett 1982), where A represents the effects of the density structure and the ^{56}Ni distribution. Here, we assume for sake of simplicity a uniform mixing of ^{56}Ni in the SN ejecta. Also, the density structures after the SN explosions with various E are analogous. Thus, the dependence on A is negligible and we investigate the LC properties depending on κ, M_{ej} and E . The synthetic LCs obtained for the models with $(M_{\text{ej}}/M_{\odot}, E_{51}) = (5.1, 5), (4.9, 10),$ and $(4.6, 20)$ are shown in Figure 9. Figure 9 also shows the multicolor and bolometric LCs of SN 2006jc.

5.2. Comparison with Observations

The period of SN 2006jc is divided into four epochs depending on the available observations: (1) UV and optical photometries at $t < 50$ days, (2) optical and NIR photometries at $t \sim 50 - 80$ days, (3) optical photometry at $t \sim 80 - 120$ days, and (4) optical, NIR, and MIR photometries and NIR spectroscopy at $t > 120$ days.

(1) At $t < 50$ days, the IR contributions to the bolometric luminosity may well be small because the IR contribution is only $\sim 10\%$ at $t \sim 50$ days. Thus, the peak bolometric luminosity derived from the UV and optical

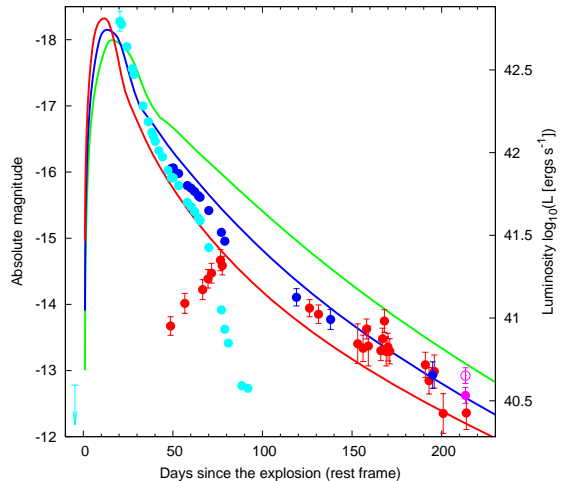


FIG. 9.— Comparison between the synthetic LCs for the models with $E_{51} = 5$ and $M_{\text{ej}} = 5.1M_{\odot}$ (green line), $E_{51} = 10$ and $M_{\text{ej}} = 4.9M_{\odot}$ (blue line), and $E_{51} = 20$ and $M_{\text{ej}} = 4.6M_{\odot}$ (red line) and the LCs of SN 2006jc ($L_{\text{UV}} + L_{\text{opt}}$: cyan filled circles, Immler et al. 2008; Kawabata et al. 2007a, 2008; Anupama et al. 2008; $L_{\text{IR,est}}(\nu < 3 \times 10^{14}\text{Hz})$: red filled circles, Arkharov et al. 2006; Di Carlo et al. 2007; L_{bol} : blue filled circles, Immler et al. 2008; Kawabata et al. 2007a, 2008; Anupama et al. 2008; Arkharov et al. 2006; Di Carlo et al. 2007; $L_{\text{IR,hot}}(\nu < 3 \times 10^{14}\text{Hz})$: magenta filled circle, Sakon et al. 2007; $L_{\text{IR}}(\nu < 3 \times 10^{14}\text{Hz})$: magenta open circle, Sakon et al. 2007). The luminosities denoted by the circles without errorbars are considerably contributed by the UV luminosity estimated as $L_{\text{UV}} = 0.8L_{\text{opt}}$.

fluxes is reliable (§ 2.1). If the bolometric LC peaked at the discovery, the peak luminosity is reproduced by the ^{56}Ni - ^{56}Co decay of $M(^{56}\text{Ni}) = 0.22M_{\odot}$. The rapid decline after the peak prefers such high-energy models as $(M_{\text{ej}}/M_{\odot}, E_{51}) = (4.9, 10)$ and $(4.6, 20)$.

(2) At $t \sim 50 - 80$ days, the IR contribution to the bolometric luminosity increases from $\sim 10\%$ at $t = 49$ days to $\sim 70\%$ at $t = 79$ days. The contribution of $L_{\text{IR,est}}(\nu < 1.3 \times 10^{14}\text{Hz})$ to $L_{\text{IR,est}}(\nu < 3 \times 10^{14}\text{Hz})$ changes from $\sim 30\%$ at $t = 49$ days to $\sim 40\%$ at $t = 79$ days. At this epoch, the optical and IR emissions contribute to the bolometric luminosities. Combining the IR brightening and the optical decline, the bolometric LC including $L_{\text{UV}} (= 0.8L_{\text{opt}})$ declines slowly. Such a slow decline is consistent with the models of $(M_{\text{ej}}/M_{\odot}, E_{51}) = (4.9, 10)$ and $(4.6, 20)$.

(3) At $t \sim 80 - 120$ days, NIR photometries are not available. The decline of the optical luminosity at this epoch is more rapid than at $t < 80$ days. Such a rapid decline of the optical LC can not be reproduced by the ^{56}Ni - ^{56}Co decay. However, the bolometric LC may well decline more slowly than the optical LC because the IR emission dominates in the bolometric luminosity.

(4) At $t > 120$ days, NIR photometries are available continuously and optical photometries are available at $t = 120, 140,$ and 195 days (Kawabata et al. 2008). The contribution of the optical emission to the bolometric luminosities is negligible ($\sim 3\%$ at $t = 120, 140,$ and 195 days). At this epoch, the contribution of $L_{\text{IR,est}}(\nu < 1.3 \times 10^{14}\text{Hz})$ to the total luminosity increases from $\sim 60\%$ at $t = 127$ days to $\sim 80\%$ at $t = 215$ days. The estimated IR luminosity is consistent with the luminosity emitted from the hot carbon dust at $t = 215$ days (§ 2.2). Since the dust temperature decreases with time, the ratio of the MIR luminosities to the NIR luminosities becomes

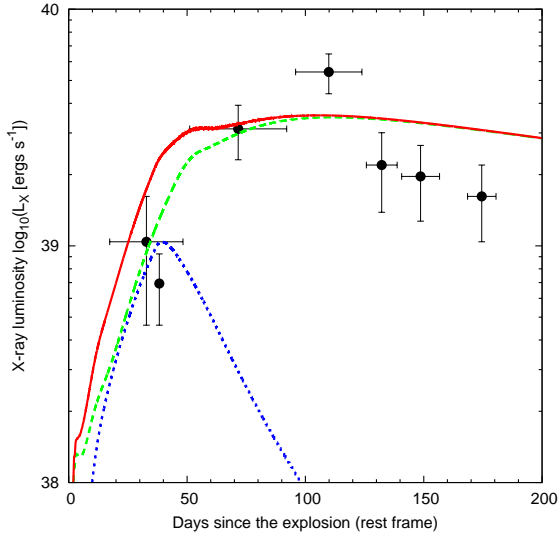


FIG. 10.— Comparison between the synthetic X-ray LCs contributed from the total emission (solid line), the SN ejecta (dashed line), and the CSM (dotted line) and the X-ray LC of SN 2006jc (circles, Immler et al. 2008).

larger with time. Therefore, the amorphous carbon emission model reasonably estimates the IR luminosity due to the hot carbon dust at $t \lesssim 215$ days. The model with $M_{\text{ej}} = 4.9M_{\odot}$, $E_{51} = 10$, and $M(^{56}\text{Ni}) = 0.22M_{\odot}$ reproduces well the LC decline at $t > 120$ days and the IR luminosities due to the hot carbon dust at $t = 215$ days¹⁶. Therefore, we conclude that the hypernova-like SN explosion model with $M_{\text{ej}} = 4.9M_{\odot}$, $E_{51} = 10$, and $M(^{56}\text{Ni}) = 0.22M_{\odot}$ is the most preferable model among the exploded models of a WCO Wolf-Rayet star with $M_{\text{preSN}} = 6.9M_{\odot}$.

6. INTERACTION WITH CIRCUMSTELLAR MATTER

X-rays from SN 2006jc were detected by the *Swift* and *Chandra* satellites (Immler et al. 2008). The X-ray detection indicates that the expanding SN ejecta collides with the CSM.

We calculate X-ray emission from the ejecta-CSM interaction for the SN model with $(M_{\text{ej}}/M_{\odot}, E_{51}) = (4.9, 10)$, and estimate the CSM density structure on the basis of a comparison with the observed X-ray LC (e.g., Suzuki & Nomoto 1995). The observed X-ray luminosities estimated with the distance of 24 Mpc in Immler et al. (2008) are scaled using 25.8 Mpc.

We adopt a CSM density profile characterized by a power-law of $\rho = \rho_0(r/r_0)^{-n}$ and assume that the interaction starts at a distance $r = 3 \times 10^{10}$ cm. The parameters ρ_0 , r_0 , and n are determined so that the ejecta-CSM interaction reproduces the observed X-ray LC.

The interaction generates reverse and forward shock waves in the SN ejecta and CSM, respectively. Both re-

¹⁶ After submission of this paper, the IR observation at $t = 425$ days was presented by Mattila et al. (2008). They estimated the total luminosity and the dust temperature as $L \sim 1.2 \times 10^{40}$ ergs s^{-1} and $T = 520$ K, respectively. Our model with $M_{\text{ej}} = 4.9M_{\odot}$, $E_{51} = 10$, and $M(^{56}\text{Ni}) = 0.22M_{\odot}$ predicted the luminosity of $L_{\text{bol}} \sim 3 \times 10^{39}$ ergs s^{-1} and the dust temperature of $T \sim 200$ K (Nozawa et al. 2008) at $t \sim 430$ days, which are lower than the observations. This suggests that the observed IR emissions at $t = 425$ days may originate not only from the newly-formed dust in the SN ejecta heated by the ^{56}Ni - ^{56}Co decay but also from the light echo of the CSM dust.

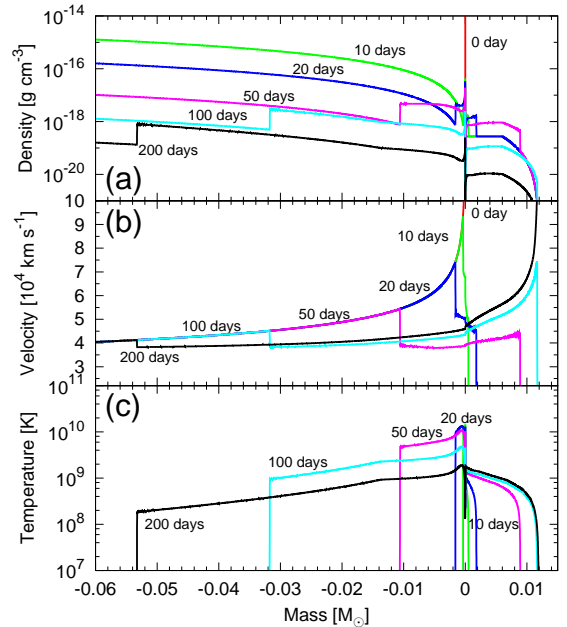


FIG. 11.— (a) Density, (b) velocity, and (c) temperature structures of the SN ejecta and the CSM at $t = 0$ day (red), 10 days (green), 20 days (blue), 50 days (magenta), 100 days (cyan), and 200 days (black). The coordinate is the Lagrangian mass with the contact discontinuity between the ejecta (left) and the CSM (right).

gions are heated by the shock waves and emit X-rays. In such a compact star, because the density in the shocked SN ejecta is higher than that in the shocked CSM, the emitted X-rays from the shocked SN ejecta are more luminous than those from the shocked CSM (Fig. 10).

Figure 10 shows the synthesized X-ray LC for $\rho_0 = 2.75 \times 10^{-19}$ g cm^{-3} and $n = 0$ for $r < 2.2 \times 10^{16}$ cm and $n = 6$ for $r > 2.2 \times 10^{16}$ cm, i.e., for a flat (inside) and steep (outside) CSM density profile of $\rho = 2.75 \times 10^{-19}$ g cm^{-3} for $r < 2.2 \times 10^{16}$ cm and $2.75 \times 10^{-19}(r/2.2 \times 10^{16}\text{cm})^{-6}$ g cm^{-3} for $r > 2.2 \times 10^{16}$ cm. The total mass of the CSM is $1.2 \times 10^{-2}M_{\odot}$ to reproduce the peak of the observed X-ray LC and the subsequent decline.

The density, velocity, and temperature structures and their evolutions are shown in Figures 11abc. The velocity of the reverse shock is $v \sim 3.8 \times 10^4$ km s^{-1} . The reverse shock reaches $\sim 5.3 \times 10^{-2}M_{\odot}$ from the outer edge of the SN ejecta at $t = 200$ days and heats up the swept-up SN ejecta. The temperature behind the reverse shock is higher than 10^8 K where dust cannot newly form and the dust formed in the SN ejecta is destroyed (Nozawa et al. 2008). Our calculation does not show the formation of a cooling shell. This is because the CSM interaction is so weak to emit X-ray of $\sim 3 \times 10^{39}$ ergs s^{-1} . If the bolometric luminosity is powered by the CSM interaction, i.e., if the CSM interaction emits as high luminosity as $\sim 8 \times 10^{42}$ ergs s^{-1} , the cooling shell might form and thus the dust formation might be possible. Further detailed studies, however, are required to confirm the dust formation behind the reverse shock.

Such a flat density profile of the inner CSM implies that the stellar wind was not steady because the steady wind should form the CSM of $\rho \propto r^{-2}$. This circumstellar environment might have been formed by a variable mass-loss rate \dot{M} and/or a variable wind velocity v_w . For example, assuming that the stellar wind blew with

a constant $v_w = 3,500 \text{ km s}^{-1}$ for two years before the explosion, the mass-loss rate must have changed from 1×10^{-2} to $2 \times 10^{-14} M_\odot \text{ yr}^{-1}$ in two years. Such a drastic change of the mass-loss rate and/or the wind velocity is consistent with the fact that the progenitor of SN 2006jc was surrounded by the matter ejected by the LBV-like event two years before the explosion.

7. CONCLUSIONS

We present a theoretical model for SN 2006jc whose properties are summarized as follows.

(1) **WCO progenitor and Dust Formation:** The progenitor is a WCO Wolf-Rayet star whose total mass has been reduced from $M_{\text{ms}} = 40M_\odot$ to as small as $M_{\text{preSN}} = 6.9M_\odot$. The WCO star model has a thick C-rich envelope and CSM. This is consistent with the formation of amorphous carbon grains in the SN ejecta and the CSM suggested by AKARI observations (Sakon et al. 2007). Nozawa et al. (2008) have calculated dust formation in the WCO star explosion model and shown that carbon dust is formed in the C-rich layer at $t \sim 50$ days. This is much earlier than the dust formation after $t \sim 1 \text{ yr}$ in Type II SNe (SNe II), because of the much smaller M_{ej} in the WCO star than SNe II. According to the models in Limongi & Chieffi (2006), the stars with $M_{\text{ms}} > 40M_\odot$ typically become WCO stars to form a thick C-rich layer and CSM. This limiting mass, however, is still uncertain and strongly depends on many details of the stellar evolution. The early dust formation in the SN ejecta and the CSM suggests that the progenitor of SN 2006jc is a massive star becoming a WCO Wolf-Rayet star.

(2) **Explosion and Bolometric Light Curve:** The multicolor LCs of SN 2006jc show peculiar evolutions, e.g., a rapid decline of the optical LC and brightening of the IR LC. These can be interpreted as an ongoing dust formation. Assuming the absorbed optical light is re-emitted in the IR band, the bolometric LC is constructed as a summation of L_{UV} ($= 0.8L_{\text{opt}}$), L_{opt} , and L_{IR} . By calculating the hydrodynamics, nucleosynthesis, and the bolometric LC for the SN explosion with the various explosion energies, $E_{51} = 1, 5, 10,$ and 20 , we find that the hypernova-like SN explosion model with $M_{\text{ej}} = 4.9M_\odot$, $E_{51} = 10$, and $M(^{56}\text{Ni}) = 0.22M_\odot$ best reproduces the bolometric LC of SN 2006jc with the radioactive decays. Also, the temperature evolution of the carbon dust heated by the ^{56}Ni - ^{56}Co decay reasonably well explains the IR observations for $t \sim 50 - 220$ days (Nozawa et al. 2008).

(3) **CSM Interaction and X-ray Light Curve:** Applying the model with $M_{\text{ej}} = 4.9M_\odot$ and $E_{51} = 10$, we calculate the ejecta-CSM interaction and the resultant X-ray LC. We derive the CSM density structure to reproduce the X-ray LC of SN 2006jc as $\rho = 2.75 \times 10^{-19} \text{ g cm}^{-3}$ for $r < 2.2 \times 10^{16} \text{ cm}$ and $2.75 \times 10^{-19} (r/2.2 \times 10^{16} \text{ cm})^{-6} \text{ g cm}^{-3}$ for $r > 2.2 \times 10^{16} \text{ cm}$. The flat density distribution in the inner CSM indicates a drastic change of the mass-loss rate and/or the wind velocity that is consistent with the LBV-like event two years before the explosion.

8. DISCUSSION

LBV connection: Our model does not take into account the LBV-like event that occurred two years before the explosion. The first reason is that the mechanism of the outburst is still unclear. The second reason is that, at least in the framework of the current understanding of standard stellar evolution, the envelope of a massive star practically freezes out after core He exhaustion (i.e., about 10000 years before the explosion) due to the more rapid evolution of the core than the envelope. In addition, it is interesting to note that, and this is a confirmation of the theoretical expectation, there is no observational evidence that any Wolf-Rayet star has ever undergone such a luminous outburst (Humphreys et al. 1999). Hence, there is no specific reason to associate the occurrence of a LBV-like outburst to the presupernova evolution. Future studies on the mechanism of the outburst are required to firmly conclude the origin of the LBV-like outburst. It would be possible that a possible binary companion star could undergo the LBV-like outburst.

Fallback: According to our hydrodynamics and nucleosynthesis calculations, in the spherically symmetric models with $E_{51} \geq 5$, the fallback does not take place and thus the amount of synthesized ^{56}Ni is much larger than $M(^{56}\text{Ni}) = 0.22M_\odot$ which is required to power the LC of SN 2006jc (§ 5.1). In the aspherical explosions, however, the fallback takes place even for $E_{51} \geq 5$. In this paper, we assume the fallback even for the models with $E_{51} \geq 5$ and derive the amount of fallback to yield the appropriate amount of ^{56}Ni . To justify the above assumption, we calculate an aspherical explosion induced by a jet with an opening angle of $\theta = 45^\circ$ and an energy deposition rate of $\dot{E} = 3 \times 10^{52} \text{ ergs s}^{-1}$ (Tominaga et al. 2007a; Tominaga 2007). The jet-induced model realizes an explosion with $M_{\text{ej}} \sim 4.9M_\odot$, $E_{51} \sim 10$, and $M(^{56}\text{Ni}) \sim 0.22M_\odot$ that is consistent with the adopted model. We note that an aspherical radiative transfer calculation is required to confirm that the jet-induced explosion model can reproduce the LC of SN 2006jc.

Light curve models: The model with $M_{\text{ej}} = 4.9M_\odot$, $E_{51} = 10$, and $M(^{56}\text{Ni}) = 0.22M_\odot$ is not an unique model to reproduce the bolometric LC of SN 2006jc. In the case of usual SNe, the velocities of the absorption lines can disentangle the degeneracy of M_{ej} and E by means of the comparison with the photospheric velocities (e.g., Tanaka et al. 2008). However, the spectra of SN 2006jc are dominated by He emission lines and the nature is unclear. Thus we cannot fully resolve the degeneracy. Since the LC shape is proportional to $M_{\text{ej}}^{3/4} E^{-1/4}$, the model with a larger M_{ej} requires a higher E . An explosion of the progenitor star with a larger M_{preSN} reproduces the LC of SN 2006jc with a higher E and the X-ray LC with a lower CSM density. On the other hand, an explosion of the progenitor star with a smaller M_{preSN} reproduces the LC with a lower E , e.g., an explosion with $M_{\text{ej}} = 1.5M_\odot$ and $E_{51} = 1$ can explain the LC shape of SN 2006jc. However, such low E explosions suppress explosive nucleosynthesis and enhance the fallback. As a result, the ^{56}Ni production is reduced for a small M_{preSN} . If the LC of SN 2006jc is powered by the ^{56}Ni - ^{56}Co decay, the bright peak indicates a larger

amount of ^{56}Ni production ($\sim 0.22M_{\odot}$) than a normal SN [$M(^{56}\text{Ni}) \sim 0.07M_{\odot}$, e.g., SN 1987A, Blinnikov et al. 2000]. Therefore, SN 2006jc is likely a more energetic explosion than a normal SN with $E_{51} \sim 1$.

Dust formation: We assume that the energy source of the LC of SN 2006jc is the ^{56}Ni - ^{56}Co decay. This consistently explains the formation of carbon dust at the early epoch ($t \sim 50$ days) and the dust temperature at $t \sim 200$ days (Nozawa et al. 2008). In this scenario, however, the origin of the bright blue continuum remains an unsolved problem (e.g., Pastorello et al. 2007; Smith et al. 2008; Immler et al. 2008). Such a spectrum might be explained by the ejecta-CSM interaction. In this scenario, however, the fine tunings are required to reproduce the bolometric LC; most of the X-rays are absorbed and converted to the optical luminosity, which only a small fraction of the X-rays are emitted with changing the fraction from 10^{-3} at $t \sim 30$ days to 0.1 at $t \sim 180$ days. Moreover, the formation of carbon dust with two temperatures would not be explained. Since both scenarios are inconclusive so far, further investigations may give important implications on the emission

mechanism of SN 2006jc.

We would like to thank A. Arkharov, N. Efimova, A. Di Paola, C. Corsi, E. Di Carlo, and M. Dolci for providing us the data of the JHK-band photometries. We also would like to thank S. Immler for the preprint on the Swift observations. M.L. thanks the support from the 21st Century COE Program (QUEST) of JSPS (Japan Society for the Promotion of Science) for his stay in the University of Tokyo and the hospitality of the Department of Astronomy. G.C.A., D.K.S., and T.P.P. are supported by the JSPS - INSA (Indian National Science Academy) exchange programme. N.T. and M.T. are supported through the JSPS Research Fellowship for Young Scientists. This work has been supported in part by World Premier International Research Center Initiative (WPI Initiative), MEXT, Japan, and by the Grant-in-Aid for Scientific Research of the JSPS (10041110, 10304014, 11740120, 12640233, 14047206, 14253001, 14540223, 16740106, 18104003, 18540231, 20540226) and MEXT (19047004, 20040004, 20041005, 07CE2002).

REFERENCES

- Anupama, G.C., et al. 2008, in preparation
 Arkharov, A., Efimova, N., Di Paola, A., Di Carlo, E., & Dolci, M. 2006, *Astron. Tel.*, 961, 1
 Arnett, W. D. 1982, *ApJ*, 253, 785
 Aufderheide, M. B., Baron, E., & Thielemann, F.-K. 1991, *ApJ*, 370, 630
 Benetti, S., et al. 2006, *Cent. Bur. Electron. Tel.*, 674, 2
 Blinnikov, S., Lundqvist, P., Bartunov, O., Nomoto, K., & Iwamoto, K. 2000, *ApJ*, 532, 1132
 Brown, P.J., Immler, S., & Modjaz, M. 2006, *Astron. Tel.*, 916, 1
 Colella, P., & Woodward, P.R. 1984, *J. Comput. Phys.*, 54, 174
 Crots, A., Eastman, J., Depoy, D., Prieto, J.L., & Garnavich, P. 2006, *Cent. Bur. Electron. Tel.*, 672, 1
 de Jager, C., Nieuwenhuijzen, H., & van der Hucht, K. A. 1988, *A&AS*, 72, 259
 Deng, J., Tominaga, N., Mazzali, P.A., Maeda, K., & Nomoto, K. 2005, *ApJ*, 624, 898
 Di Carlo, E., et al. 2007, *ApJ*, submitted (arXiv:0712.3855)
 Eldridge, J. J., & Vink, J. S. 2006, *A&A*, 452, 295
 Fesen, R., Milisavljevic, D., & Rudie, G. 2006a, *Cent. Bur. Electron. Tel.*, 672, 2
 Foley, R. J., Smith, N., Ganeshalingam, M., Li, W., Chornock, R., & Filippenko, A. V. 2007, *ApJ*, 657, L105
 Holland, S., et al. 2007, "Supernova 1987A: 20 Years After: Supernovae and Gamma-Ray Bursters", ed. S. Immler, K.W. Weiler, and R. McCray (AIP: New York), in press. The poster paper is available at <http://astrophysics.gsfc.nasa.gov/conferences/supernova1987a/Holland-poster.pdf>
 Humphreys, R. M., Davidson, K., & Smith, N. 1999, *PASP*, 111, 1124
 Immler, S., Modjaz, M., & Brown, P. J. 2006, *Astron. Tel.*, 934, 1
 Immler, S., et al. 2008, *ApJ*, 674, L85
 Iwamoto, K., et al. 2000, *ApJ*, 534, 660
 Janka, H.-Th., Langanke, K., Marek, A., Martínez-Pinedo, G., & Müller, B. 2007, *Phys. Rep.*, 442, 38
 Kawabata, K. S., Maeda, K., Tanaka, M., Tominaga, N., Nomoto, K., & Hattori, T. 2007a, *IAU Circ.*, 8833, 3
 Kawabata, K. S., et al. 2008, in preparation
 Langer, N. 1989, *A&A*, 220, 135
 Limongi, M., & Chieffi, A. 2003, *ApJ*, 592, 404
 Limongi, M., & Chieffi, A. 2006, *ApJ*, 647, 483
 Maeda, K., & Nomoto, K., 2003, *ApJ*, 598, 1163
 Maeda, K., et al. 2007, *ApJ*, 658, L5
 Maeder, A., & Meynet, G. 2003, *A&A*, 404, 975
 Matheson, T., Filippenko, A. V., Chornock, R., Leonard, D. C., & Li, W. 2000, *AJ*, 119, 2303
 Mattila, S., et al. 2008, *MNRAS*, in press (arXiv:0803.2145)
 Mazzali, P. A., et al. 2006, *Nature*, 442, 1018
 Mazzali, P. A., et al. 2007, *ApJ*, 661, 892
 Meynet, G., & Maeder, A. 2003, *A&A*, 404, 975
 Minezaki, T., Yoshii, Y., & Nomoto, K. 2007, *IAU Circ.*, 8833, 2
 Minezaki, T., et al. 2008, in preparation
 Modjaz, M., Blondin, S., Kirshner, R., Challis, P., Matheson, T., & Mamajek, E. 2006a, *Cent. Bur. Electron. Tel.*, 676, 1
 Modjaz, M., Blondin, S., Kirshner, R., Challis, P., Matheson, T., & Mamajek, E. 2006b, *Cent. Bur. Electron. Tel.*, 677, 1
 Nakano, S. et al. 2006, *Cent. Bur. Electron. Tel.*, 666, 1
 Nomoto, K. 1982, *ApJ*, 253, 798
 Nomoto, K., & Hashimoto, M. 1988, *Phys. Rep.*, 163, 13
 Nomoto, K., Tominaga, N., Umeda, H., Kobayashi, C., & Maeda, K. 2006, *Nucl. Phys. A*, 777, 424 (astro-ph/0605725)
 Nozawa, T., Kozasa, T., Umeda, H., Maeda, K., & Nomoto, K. 2003, *ApJ*, 598, 785
 Nozawa, T., et al. 2008, *ApJ*, in press (arXiv:0801.2015)
 Nugis, T., & Lamers, H. J. G. L. M. 2000, *A&A*, 360, 227
 Pastorello, A., et al. 2007, *Nature*, 447, 829
 Pian, E., et al. 2006, *Nature*, 443, 1011
 Sakon, I., et al. 2007, *ApJ*, submitted (arXiv:0711.4801)
 Schlegel, D. J., Finkbeiner, D. P., & Davis, M. 1998 *ApJ*, 500, 525
 Smith, N., Foley, R. J., & Filippenko, A. V. 2008, *ApJ*, in press (arXiv:0704.2249)
 Soderberg, A. 2006, *Astron. Tel.*, 917, 1
 Sugimoto, D., & Nomoto, K. 1975, *Sci. Pap. Coll. Gen. Educ. Univ. Tokyo*, 25, 109
 Suzuki, T., & Nomoto, K. 1995, *ApJ*, 455, 658
 Tanaka, M., et al. 2008, *ApJ*, submitted (arXiv:0807.1674)
 Tominaga, N., Maeda, K., Umeda, H., Nomoto, K., Tanaka, M., Iwamoto, N., Suzuki, T. & Mazzali, P. 2007a, *ApJ*, 657, L77
 Tominaga, N., Umeda, H., & Nomoto, K. 2007b, *ApJ*, 660, 516
 Tominaga, N. 2007, *ApJ*, submitted (arXiv:0711.4815)
 Turatto, M., Cappellaro, E., Danziger, I. J., Benetti, S., Gouiffes, C., & Della Valle, M. 1993, *MNRAS*, 262, 128
 Turatto, M., et al. 2000, *ApJ*, 534, L57
 Umeda, H., & Nomoto, K. 2005, *ApJ*, 619, 427
 Vink, J. S., de Koter, A., & Lamers, H. J. G. L. M. 2000, *A&A*, 362, 295
 Woosley, S. E., & Weaver, T. A. 1995, *ApJS*, 101, 181
 Yoshii, Y., et al. 2003, *ApJ*, 592, 467